Experiment and Analysis of Laser Oscillation and Atomic Processes in Positive-Column He-Cd Discharge

By

Yoshiro OGATA* and Kuniya FUKUDA**

(Received March 31, 1975)

Abstract

The observations of the 4416 Å laser output power and spontaneous emission of several Cd^+ spectral lines, as well as the measurements of electron temperature and density are carried out on the positive-column He-Cd^+ laser discharge (3.2 mm main bore). Further, the plasma balance equation is extended to a mixture gas in the free fall as well as in the ambipolar diffusion, and then applied to the He-Cd^+ laser plasma with the consideration of the mean free paths of He and Cd ions in the plasma of the binary mixture. The equation is solved under the typical conditions for lasing, (He pressure of 4 Torr, discharge current of 120 mA and evaporator temperature of 190 to 260°C), in combination with the population densities derived from our previous experiment. The results give the total number density of Cd ions and all the rates for ionization in the plasma. Then, the various rates for the population to the 4416 Å laser lower level are estimated and discussed in relation to the oscillation mechanism of the laser, especially with regard to the population process of the laser lower level.

§1. Introduction

Silfvast[1] and Browne *et al.*[2] have proposed that in the CW He-Cd^+ laser, the upper levels of the laser transitions 4416 Å and 3250 Å are excited mainly by the Penning collisions of ground level Cd atoms with metastable He atoms. The present authors[3] recently have proved definitely the dominance of the Penning collisions by the hook method.

The aim of the present work is to make clear the oscillation mechanism of the 4416 Å laser in the He-Cd positive column. For this purpose, in general, it is necessary to know the excitation and de-excitation processes of the laser

* Department of Mechanical Engineering II. Present address: Research Laboratory, Matsushita Electronics Corporation, Takatsuki, Osaka.

** Department of Engineering Science.

upper and lower levels. The excitation mechanisms of the lower levels are not yet examined in detail, although Browne *et al.*[2] and Giallorenzi[4] suggested that the lower levels do not play any role in the oscillation.

In section 2, first the spontaneous emissions from the 4416 Å upper and lower levels are observed simultaneously with the laser output power for various discharge conditions, especially for the varied evaporator temperature so that the inversion mechanism is examined. The spontaneous emissions of various Cd^+ lines are also observed to discuss the population processes of the laser lower level. Further, the experiments with probes are made on the He-Cd^+ laser plasma to get the values of plasma parameters, *i.e.*, electron temperature and density, which enable us to perform the analysis in the following section.

For a binary mixture, Dorgela *et al.*[5] have extended Engel's formula[6] which is based on Schottky's analysis[7] to a binary mixture in the case in which the ambipolar diffusion is effective. Further, Young *et al.*[8] applied the work of Dorgela *et al.*[5] to the He-Na laser discharge. In section 3, general formulae for the plasma balance equations are newly introduced for a mixture gas in the free fall[9], as well as in the ambipolar diffusion[7].

In section 4, it is proved that the ambipolar diffusion is valid for the He-Cd^+ laser plasma in the experiments of section 2, and then the wall recombination rates are given. Furthermore, the various rate coefficients for the ionization by electron collision as well as by the Penning collision are shown for the He-Cd plasma, in which stepwise ionization is dominant.

In section 5, the calculation is performed by making use of the formula for recombination and ionization given in section 4, and the values of the various ionization rates are shown. Then, the population and depopulation mechanism of the laser lower level is analyzed.

§2. Experimentals

2-1 Laser output power and spontaneous emission

The 4416 Å laser output power and spontaneous emissions of several Cd^+ lines were observed for various discharge conditions in the dc cataphoretic type laser tubes of main bore $d=3.2$ mm. The energy level diagrams of Cd, Cd^+ and He are shown in Fig. 1 together with the transitions of interest.

Figure 2 shows the 4416 Å laser output power as a function of discharge current for various filling gas pressures p. In this measurement, the laser resonator was 1.5 m in length and was composed of two mirrors with a 2 m radius of curvature, the reflectivities of which are 98 and 100% at 4416 Å. The eva-

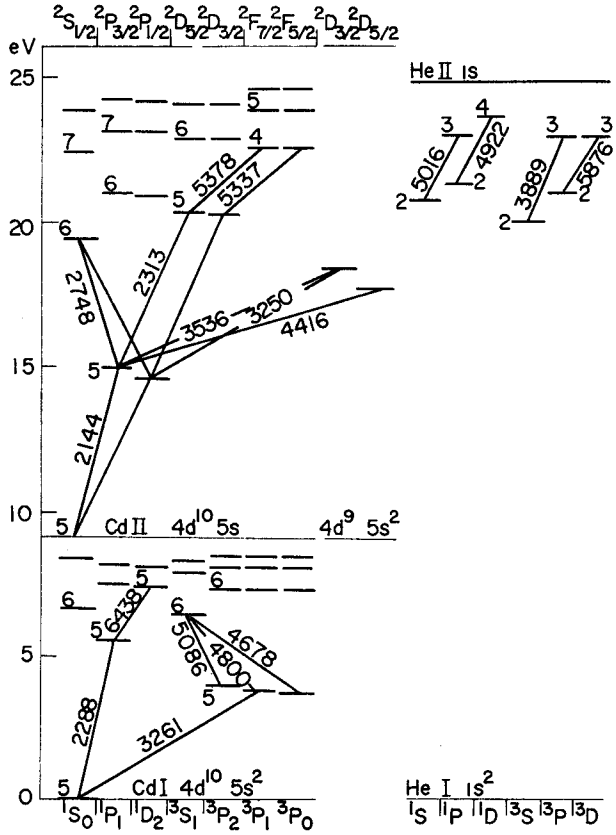

Fig. 1. Energy level diagrams of Cd, Cd^+ and He.

porator temperature T_{ev} was kept at 262±2°C. The laser capillary was 800 mm in length and made of a thick-wall Pyrex tube. The capillary wall was heated by heating tape at the constant temperature T_w=370±5°C. The output power was measured by a solar cell with an accuracy within ten percent error.

Figure 3 shows the 4416 Å laser output power as a function of T_{ev} with parameter I. In this measurement, the laser resonator was 1.18 m in length and was composed of two mirrors with a 2.5 m radius of curvature, the reflectivities of which were 99 and 100% at 4416 Å. The value of p was 4 Torr. The laser capillary was 500 mm in length and made of a thick-wall fused quartz. The capillary wall was also heated by heating tape at the constant temperature T_w =370±5°C. The output power was measured with a photomultiplier tube, and the unit of the measured value is arbitrary in the figure.

From the above experimental results, it is obvious that the 4416 Å laser oscillates most intensively under the following conditions: p=3~4 Torr, $T_{ev}\simeq$240

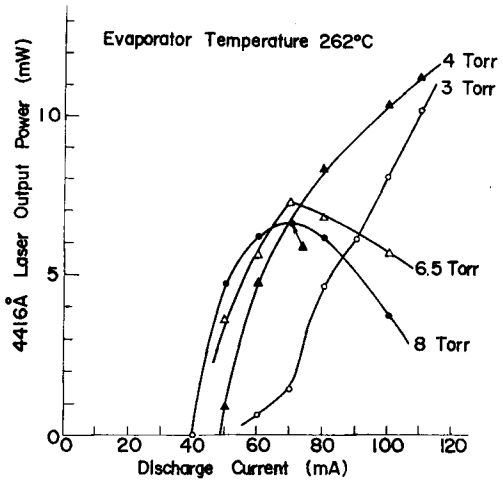

Fig. 2. 4416 Å laser output power as a function of discharge current for various He pressures in the capillary of 3.2 mm main bore. The mirror reflectances are 98 and 100 %.

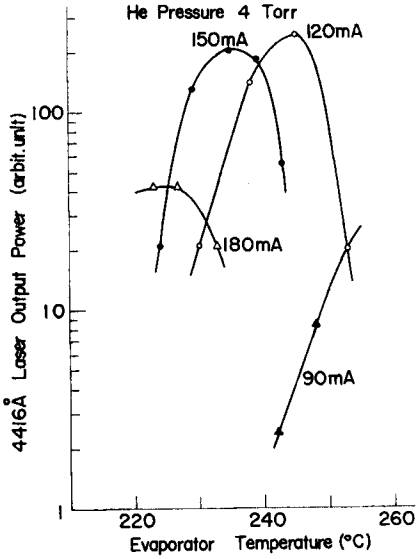

Fig. 3. Variation of 4416 Å laser output power as a function of evaporator temperature for various discharge currents in the capillary of the same bore as in Fig. 2. The mirror reflectances are 99 and 100 %.

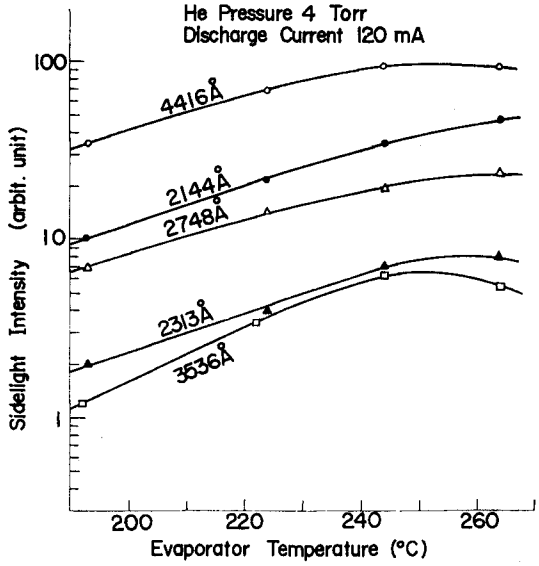

Fig. 4. Variation of Cd^+ spontaneous emission from the capillary of the same main bore as in Fig. 2.

°C and $I \simeq 120$ mA. The optimum value of the product pd is about 10 Torr•mm, which is quite similar to the results of the previous investigations[1,10].

Figure 4 shows the spontaneuos emission intensity of the various Cd^+ lines in the laser plasma as a function of T_{ev}, where the transitions concerned are shown in Fig. 1. As the 4416 Å emission is considered to be optically thin[11], the sidelight intensity of the emission is proportional to the population density n_u of the laser upper level. From Figs. 3 and 4, it is seen that for 120 mA, n_u has a maximum value at $T_{ev} \simeq 245$°C. The 2144 Å sidelight intensity is proportional to the population density n_l of the 4416 Å lower level, since we assume that the radiation is not imprisoned in spite of the relatively large transition probability[12]. (See the last section.) In Fig. 4, it is seen that the 2144 Å sidelight intensity increases monotonously with the increase of T_{ev}, while the sidelight intensity of other lines tends to saturate or decrease at some value of T_{ev}.

From Figs. 3 and 4, the oscillation mechanism is explained as follows. While T_{ev} is low ($\lesssim$230°C), n_u is so small that the inversion density is lower than the threshold and the laser does not oscillate. As T_{ev} increases, the inversion density exceeds the threshold and the laser begins to oscillate. When T_{ev} increases up to 245°C, the inversion density reaches a maximum and the laser output power has a maximum. As T_{ev} increases higher than 245°C, n_u begins to decrease slowly and n_l continues to increase. Therefore, the inversion density, and hence the output power, begins to decrease.

As already mentioned in previous works[2,3], the dominant process of population to the 4416 Å upper level is the Penning collisions of ground level Cd atoms with metastable He atms. On the other hand, the population processes of the 4416 Å lower level is not yet examined. If the lower level were predominantly populated by the radiative cascading from the laser upper level, the 2144 Å emission would behave similarly to the 4416 Å emission. But as seen in Fig. 4, the 2144 Å sidelight intensity increases monotonously with the increase of T_{ev}, in contrast to the saturation of the 4416 Å sidelight intensity. Figure 4 also shows that the 4416 Å lower level is not populated predominanlty from the $5s^2\ ^2D_{3/2}$, $6^2S_{1/2}$ and $5^2D_{5/2}$ levels by the radiative cascadings of the 3536 Å, 2748 Å and 2313 Å lines, respectively (also see refs. 3 and 13).

2-2 Measurement of electron temperature and density

A double probe method[14] was used to evaluate the plasma parameters, *i.e.*, electron temperature T_e and electron density n_e. The experimental procedures are as follows.

Pairs of double probes were sealed 100 mm apart from each other in the

center of a thick-wall Pyrex discharge tube of the same main bore as presented in the preceding paragraph. The double probe was made from two cylindrical tungsten wires with a 0.2 mm outer diameter and a 4 mm length, facing each other 1.5 mm apart along the tube axis.

We evaluated T_e by the method[15] which was concerned with the asymmetry in V-i characteristics of the probe. We evaluated n_e by the method[16] in which the potential distribution through the sheath of the probe was analyzed exactly.

Furthermore, the electrical conductivity of plasma[17] was measured to check the above obtained values of the plarameters. Because the electrons are scattered dominantly by He atoms in the He-Cd discharge, the approximated formula of electrical conductivity[18] is applicable to get the value of n_e from the measured conductivity for a value of T_e obtained by the probe method.

The measurements were carried out under the typical condition for the laser oscillation, that it, p=4 Torr, T_w=370°C and T_{ev}=242°C, and also under

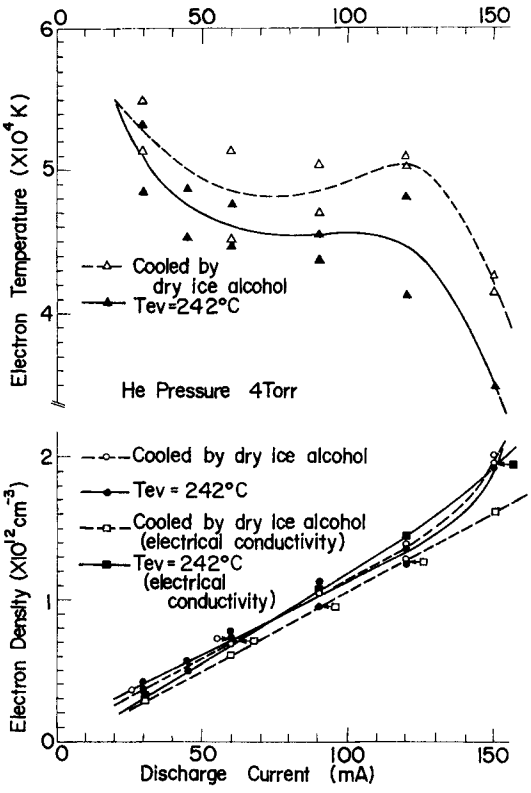

Fig. 5. Electron temperature and electron density of the He-Cd plasma in the capillary of the same bore as in Fig. 2.

the same condition, except that the evaprorator was cooled by dry ice alcohol. The obtained values of T_e and n_e are shown in Fig. 5. The results are as follows.

1. The values of n_e determined by the double probe method are almost equal to the values derived from the electrical conductivity of the plasma.
2. Both the n_e and T_e values are almost equal to the values[19,20] so far obtained under the discharge conditions close to the present ones.
3. The electron density n_e is proportional to the discharge current I.
4. The electron density n_e is almost independent on T_{ev}.
5. As I increases, that is, as n_e increases, T_e decreases.
6. As T_{ev} increases, that is, as the density of Cd atoms increases in the capillary, T_e decreases a little.
7. The value of T_e for the discharge in pure He gas agrees fairly well with the one derived from the calculation[21].

§3. Plasm Balance Equations for Mixture Gas in Positive Column

The formulae for the plasma particle balance in the positive column have been established in the case of a steady state discharge of one component gas[7,9]. This section is concerned with the plasma particle balance for mixture gas in the positive column.

In the free fall model of a binary mixture, the original formula[9] for the plasma particle balance may be modified as follows. The Poisson equation is solved by the same procedures as in the case of the original one[9]. Then, the adjustable constant is modified as

$$\alpha=\sum_{i=1}^{2} Z_i(M_i/2kT_e)^{1/2}, \tag{1}$$

which normalizes the radial distance from the axis to the wall of the column, where Z_i is the number of ion i generated by electron collisions in unit time, M_i is the mass of ion i, k is the Boltzmann constant and T_e is the electron temperature. Hence, the generalized condition that the potential gradient is infinite at the wall of the column leads Eq. (1) to the balance equation,

$$\sum_{i=1}^{2} \frac{Z_i}{\gamma_{F,i}}=1, \tag{2}$$

where $\gamma_{F,i}$ is the wall recombination rate of ion i and described as

$$\gamma_{F,i}=\frac{0.772}{R}\left(\frac{2kT_e}{M_i}\right)^{1/2}, \qquad i=1 \text{ and } 2 \tag{3}$$

for the radius R of the column.

For the ambipolar diffusion in a binary mixture, Engel's assumption[6] holds that the net number of ions which diffuse in unit time from the volume element dr at the radial distance r from the tube axis per unit length to the wall of the column, is equal to the number of ions generated by electrons unit time in the volume element. Therefore, the following equation may be written for ion 1 and 2;

$$\frac{d^2n_i^+}{dr^2}+\frac{1}{r}\frac{dn_i^+}{dr}+\frac{Z_i}{D_{a,i}}n_e=0 \qquad \text{for } i=1 \text{ and } 2, \tag{4}$$

where n_i^+ is the number density of ion i in unit volume, and $D_{a,i}$ is the ambipolar diffusion coefficient of ion i. The addition of Eqs. (4) with $i=1$ and 2 under the neutrality condition $n_1^+ + n_2^+ = n_e$ leads to the equation for the radial distribution,

$$\frac{d^2n_e}{dr^2}+\frac{1}{r}\frac{dn_e}{dr}+\left(\frac{Z_1}{D_{a,1}}+\frac{Z_2}{D_{a,2}}\right)n_e=0. \tag{5}$$

The solution is a Bessel function of zeroth order

$$\frac{n_e}{n_{e0}}=J_0\left(r\sqrt{\frac{Z_1}{D_{a,1}}+\frac{Z_2}{D_{a,2}}}\right), \tag{6}$$

where n_{e0} is the number density of electrons at the axis of the column. Then, following the procedures of ref. 6, we can obtain the plasma balance equation,

$$R\sqrt{\frac{Z_1}{D_{a,1}}+\frac{Z_2}{D_{a,2}}}=2.405. \tag{7}$$

The ambipolar diffusion coefficients are given as

$$D_{a,i}=\frac{kT_e}{e}\frac{760}{p}\mu_i \qquad \text{for } i=1 \text{ and } 2, \tag{8}$$

where e is the electronic charge, p is the filling gas pressure, and μ_i is the mobility of ion i at 760 Torr and 300 K. The μ's are evaluated by application of Blanc's law and given as

$$\frac{1}{\mu_i}=\sum_{j=1}^{2}\frac{f_j}{\mu_{ij}} \qquad \text{for } i=1 \text{ and } 2, \tag{9}$$

where f_j is the ratio of the partial pressure of gas j to the total pressure, μ_{ij} is the mobility of ion i in gas j. In combination with Eq. (8), Eq. (7) is rewritten as

$$\sum_{i=1}^{2}\frac{Z_i}{\gamma_{A,i}}=1, \tag{10}$$

where $\gamma_{A,i}$ is the wall recombination rate of ion i and described as

$$\gamma_{A,i}=\left(\frac{2.405}{R}\right)^2\frac{T_e}{11600}\frac{760}{p}\mu_i \qquad \text{for } i=1 \text{ and } 2. \tag{11}$$

Thus, the original formulae for the plasma particle balance have been extended to a binary mixture gas in the free fall, as well as in the ambipolar diffusion. The formulae for the plasma balance are simply described by the ionization rates Z's and wall recombination rates γ_F's or γ_A's.

Equations (2) and (10) may be extended to a mixture gas of more than two components. For the free fall, the formula is given as

$$\sum_i \frac{Z_i}{\gamma_{F,i}}=1, \tag{12}$$

and for the ambipolar diffusion the formula is given as

$$\sum_i \frac{Z_i}{\gamma_{A,i}}=1, \tag{13}$$

where Z_i is the number of ion i generated by an electron in unit time, $\gamma_{F,i}$ or $\gamma_{A,i}$ is the wall recombination rate of ion i by free fall or ambipolar diffusion, respectively, and the summation is carried out on all the components.

§4. Plasma Particle Balance for He-Cd$^+$ Laser Plasma in the Positive Column

Now, the formulae obtained in the preceeding section are applied to the He-Cd$^+$ laser described in section 2. We are particularly interested in the discharge under the conditions of Fig. 4, that is, the main bore $d=3.2$ mm, the filling gas pressure $p=4$ Torr, the discharge current $I=120$ mA and the evaporator temperature $T_{ev}=190$ to 260°C. The population densities of several Cd, Cd$^+$ and He levels were measured in our previous experiment[3] under the same discharge conditions as the present experiment. The values are shown as a function of T_{ev} in Table 1.

4-1 Validity of ambipolar diffnsion

In the He-Cd$^+$ laser discharge, the ion of one component He$^+$ or Cd$^+$ encounters the gases of both components in the binary mixture, that is, He and Cd gases, so that the mean free path of He$^+$ or Cd$^+$ may be represented as

$$\lambda_i=\frac{1}{\sum_{j=1}^{2}\sigma_{ij}n_j} \qquad \text{for } i=1 \text{ and } 2, \tag{14}$$

where $i=1$ and 2 stand for He^+ and Cd^+, respectively. Here, n_j is the number density of gas j, and σ_{ij} is the total cross section of ion i for the collisions with gas j, where $j=1$ and 2 stand for He and Cd gases, respectively.

In Eq. (14) the maximum value $3.73\times10^{13}\,cm^{-3}$ of Cd atom density at $T_{ev}=258°C$ in Table 1 is used for n_2, and n_1 is estimated to be $5.4\times10^{16}\,cm^{-3}$ by application of the gas law to the initial gas at $p=4$ Torr under the assumption that the gas temperature T_g is about 450°C in the discharge. The value of σ_{11} is about $5\times10^{-15}\,cm^2$ [22] (charge transfer plus elastic collision), and the one of σ_{12} about $3.7\times10^{-15}\,cm^2$ [23] (charge transfer collision). We do not have any data of σ_{2j} for Cd^+, and so the value $3\times10^{-15}\,cm^2$ [22] for the elastic collisions of Cs^+ with He atoms is substituted in σ_{21}. Furthermore, it is highly probable that σ_{22} is, at most, of the order of $10^{-13}\,cm^2$. Then, the mean free paths of the ions are approximately given by

$$\left.\begin{aligned}\lambda_1\equiv\lambda_{He^+}\simeq\frac{1}{\sigma_{11}n_1}=3.7\times10^{-3}\text{ cm}\\ \text{and}\\ \lambda_2\equiv\lambda_{Cd^+}\simeq\frac{1}{\sigma_{21}n_1}=6.2\times10^{-3}\text{ cm.}\end{aligned}\right\}\qquad(15)$$

It has become clear that the mean free paths of the ions are much smaller than the radius of the column so that Eq. (10) with Eq. (11) (the formula for a binary mixture in the ambipolar diffusion) must be applied to the discharge of the present interest.

Now the ion mobilities μ_i's in Eq. (11) are estimated using Eq. (9), where $i=1$ and 2 stand for He^+ and Cd^+, respectively, and $j=1$ and 2 stand for He and Cd gases, respectively. From Eq. (15), it is recognized that both He^+ and Cd^+ diffuse towards the tube wall without interception by Cd atoms. Therefore, the mobilities are also given by

$$\mu_i=\mu_{i1}\qquad\text{for } i=1\text{ and }2.\qquad(16)$$

In the present calculation, the value of μ_{11} is 10.4[24], and the one of μ_{21} is estimated to be 20.0 from the value of the ion mobility in He gas at 760 Torr, represented as a function of ion mass[25].

The mobilities may be influenced by the sheath and ion temperature effects[26]. The correction factor for the sheath effect is represented as a function of the Debye shielding length at the axis of the column and the radius R. In the present case, R of 1.6 mm and n_e of about $1.3\times10^{12}\,cm^{-3}$ (Fig. 5) lead to the correction factor of 1.26 at $T_e=40000$ K and of 1.28 at $T_e=50000$ K, so that it is assumed below to be constant, 1.27. On the other hand, the correction factor for

the ion temperature effect is represented as a function of ion temperature T_i, and estimated to be 0.734 under the assumption that T_i is equal to T_g of 450°C. Thus, the mobilities must be multiplied by the correction factor 0.93, and so we obtain $\mu_1=9.6$ and $\mu_2=19.0$.

Finally, the rates $\gamma_{A,i}$'s in Eq. (11) are written as

$$\left.\begin{aligned}&\gamma_{A,1}\equiv\gamma_{He^+}=36\times T_e\\ \text{and}\qquad&\\ &\gamma_{A,2}\equiv\gamma_{Cd^+}=70\times T_e,\end{aligned}\right\}\tag{17}$$

where T_e is given in Kelvin.

4-2 Ionization rates Z_1 and Z_2

In the discharge under consideration, He atoms are ionized not only from the ground 1^1S level ($i=1$) but also from the four lowest excited 2^3S, 2^1S, 2^3P and 2^1P levels ($i=2$ to 5)[21], so that Z_1 in Eq. (10) is expressed as

$$Z_1\equiv Z_{He}=\sum_{i=1}^{5}n_1(i)S_1(i),\tag{18}$$

where $n_1(i)$ is the population density of level i, and $S_1(i)$ is the rate coefficient for the ionization from level i.

The ionizations of Cd atoms may occur not only by the Penning collisions[1~3] with metastable He atoms, but also by the electron collisions with the ground 5^1S level and the excited levels 5^3P ($=5\sum_i{}^3P_i$ in Table 1) and 5^1P, so that Z_2 is written as

$$\begin{aligned}Z_2\equiv Z_{Cd}=&(1/n_e)n_2(5^1S)n_1^*\langle\sigma v\rangle+n_2(5^1S)S_2(5^1S)\\&+n_2(5^3P)S_2(5^3P)+n_2(5^1P)S_2(5^1P),\end{aligned}\tag{19}$$

where n_1^* is the total number density of the four lowest excited levels $i=2$ to 5 of He atom, $\langle\sigma v\rangle$ is the velocity averaged rate coefficient for the Penning ionization, $n_2(5^1S)$, $n_2(5^3P)$ and $n_2(5^1P)$ are the population densities of Cd 5^1S, 5^3P and 5^1P levels, respectively, and $S_2(5^1S)$, $S_2(5^3P)$ and $S_2(5^1P)$ are the rate coefficients for the ionizations from Cd 5^1S, 5^3P and 5^1P levels, respectively. In Z_2, the ionizations to Cd^+ $5s^2\ ^2D$ and 5^2P levels from Cd 5^1S level are excluded, because of small cross sections ($\sim10^{-17}$ cm^2)[27,28] in the range of electron energy under consideration. Moreover, the ionization from Cd 6^3S to Cd^+ 5^2S level is excluded.

Drawin's semiempirical formula[29] is employed for all the rate coefficients S_1 and S_2. In Eq. (19), $S_2(5^3P)$ is formulated with all the levels $5^3P_{0,1,2}$ being made at one level 5^3P_1, since the energy intervals among them are all smaller

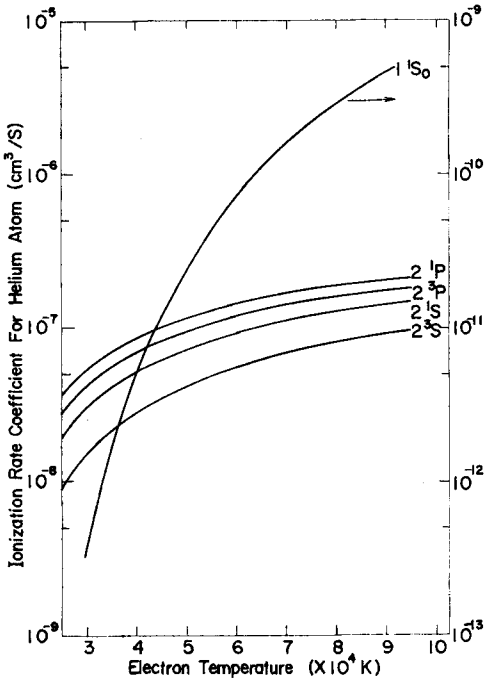

Fig. 6. Ionization rate coefficient from He ground and excited levels as a function of electron temperature. The curve for the ground 1^1S level is referred to the ordinate in the right side.

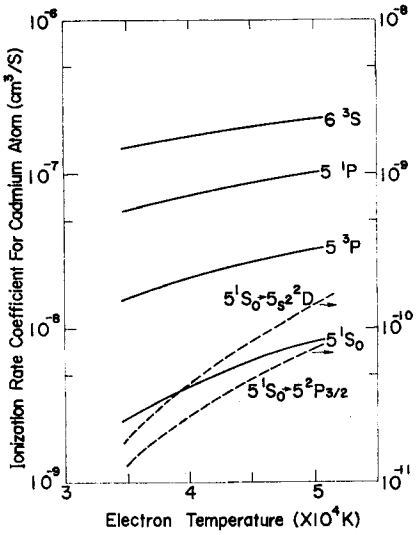

Fig. 7. Ionization rate coefficient from Cd ground and excited levels as a function of electron temperature. The curves for the transitions from the ground level to the excited $5s^2\ ^2D$ and $5^2P_{3/2}$ levels are referred to the ordinate in the right side.

than their ionization potentials. The rate coefficients S_1 and S_2 are given as a function of T_e in Figs. 6 and 7, respectively.

Since the energy dependnce of the cross section σ for the Penning ionization is not known at present, $<\sigma v>$ is assumed to be defined as the velocity averaged cross section $<\sigma>$ times the mean value of relative kinetic velocity $<v>$. In the present calculation, the value $6.5\times10^{-15}\,\mathrm{cm}^2$ [23] is used for $<\sigma>$, and $<v>$ is assumed to be 2×10^5 cm/s, corresponding to $T_g=450$°C.

§5. Results and Discussions

5-1 Electron temperature and ionization mechanism

Equation (10) together with Eqs. (17) to (19) have been numerically solved to evaluate the value of T_e as a function of T_{ev} for $n_e=1.3\times10^{12}\,\mathrm{cm}^{-3}$, corresponding to $I=120$ mA at $p=4$ Torr (see Fig. 5), where use is made of the values

Table 1.* Population densities in cm^{-3} at 4 Torr and 120 mA[3].

T_{ev} (°C)		0	169~171.5	209	229	249	258
Cd	5^1S_0	0	2.1^{12}	7.9^{12}	1.42^{13}	2.58^{13}	3.13^{13}
	5^3P_0	0	?	1.5^{11}	3.3^{11}	7.23^{11}	1.26^{12}
	5^3P_1	0	?	2.3^{11}	5.20^{11}	1.01^{12}	1.61^{12}
	5^3P_2	0	1.0^{11}	4.36^{11}	8.97^{11}	1.79^{12}	2.89^{12}
	$5\sum_i {}^3P_i$	0		8.2^{11}	1.75^{12}	3.52^{12}	5.76^{12}
	5^1P_1	0	?	?	3.12^{10}	9.6^{10}	1.91^{11}
Cd (Total)		0	?	8.72^{12}	1.63^{13}	2.94^{13}	3.73^{13}
Cd^+	$5s^2\ ^2D_{5/2}$	0	?	2.9^{10}	4.2^{10}	5.6^{10}	5.0^{10}
	$5s^2\ ^2D_{3/2}$	0	2.5^9	8.2^9	1.3^{10}	1.7^{10}	1.6^{10}
He	1^1S	5.4^{16}	5.4^{16}	5.4^{16}	5.4^{16}	5.4^{16}	5.4^{16}
	2^3S	9.5^{12}	9.6^{12}	9.26^{12}	8.2^{12}	7.2^{12}	6.4^{12}
	2^1S	1.06^{12}	1.26^{12}	1.15^{12}	1.02^{12}	9.5^{11}	7.14^{11}
	2^3P	4.9^{12}	4.9^{12}	4.7^{12}	4.36^{12}	3.84^{12}	3.27^{12}
	2^1P	9.99^{11}	1.1^{12}	1.04^{12}	9.9^{11}	9.4^{11}	8.1^{11}
He excited (Total)		1.65^{13}	1.69^{13}	1.62^{13}	1.46^{13}	1.29^{13}	1.12^{13}

* In Table 1 to 3 the indeces indicate the power of 10 by which the number is to be multiplied.

Table 2. Calculated quantities under the same discharge condition as in Fig. 4. The numbers in the parentheses indicate the percentage.

T_{ev} (°C)		0	209	229	249	258
T_e (K)		46000	45000	45000	44000	44000
n_2^+	(cm^{-3})	0	7.8^{10}	1.4^{11}	2.5^{11}	2.9^{11}
n_2^+ ($5^2S_{1/2}$)	(cm^{-3})	0	4.1^{10}	8.5^{10}	1.8^{11}	2.2^{11}
n_eZ_{Cd} ($cm^{-3}\ s^{-1}$)	Penning col.	0	1.66^{17} (64)	2.70^{17} (60)	4.34^{17} (57)	4.52^{17} (50)
	e⁻ col. (5^1S_0)	0	6.4^{16} (25)	1.14^{17} (25)	1.95^{17} (26)	2.47^{17} (27)
	e⁻ col. (5^3P)	0	2.9^{16} (11)	6.1^{16} (14)	1.2^{16} (16)	1.95^{17} (21)
	e⁻ col. (5^1P)	0		3.5^{15} (1)	1.1^{15} (1)	2.2^{16} (2)
	Total	0	2.59^{17} (100)	4.50^{17} (100)	7.26^{17} (100)	9.17^{17} (100)
n_eZ_{He} ($cm^{-3}\ s^{-1}$)	1^1S	9.5^{17} (44)	8.5^{17} (42)	8.5^{17} (44)	7.0^{17} (43)	7.0^{17} (46)
	2^3S	4.4^{17} (21)	4.2^{17} (21)	3.8^{17} (20)	3.3^{17} (20)	2.3^{17} (19)
	2^1S	9.4^{16} (4)	9.5^{16} (5)	8.3^{16} (4)	7.5^{16} (5)	5.9^{16} (4)
	2^3P	5.5^{17} (25)	5.1^{17} (25)	4.7^{17} (25)	4.0^{17} (25)	3.5^{17} (23)
	2^1P	1.3^{17} (6)	1.3^{17} (7)	1.3^{17} (7)	1.2^{17} (7)	1.1^{17} (7)
	Total	2.16^{18} (100)	1.99^{18} (100)	1.90^{18} (100)	1.63^{18} (100)	1.51^{18} (100)

of the population densities in Table 1. Furthermore, the first and second terms on the left side of Eq. (10) times n_e, that is, $(Z_1/\gamma_{A,1})n_e$ and $(Z_2/\gamma_{A,2})n_e$, become the number density n_1^+ of He^+, and the number density n_2^+ of Cd^+, respectively.

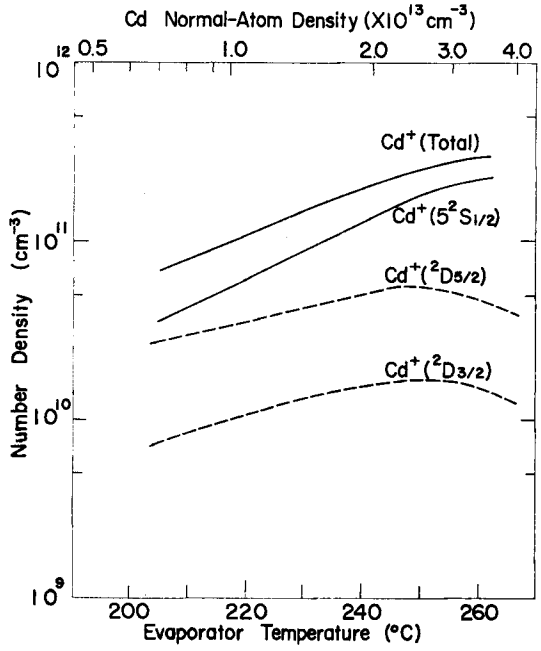

Fig. 8. Total number density of Cd^+ and population densities of various Cd^+ levels under the same discharge condition as in Fig. 4.

Then, the number density $n_2^+(5^2S_{1/2})$ of the Cd^+ ground $5^2S_{1/2}$ level is determined by subtracting the number densities of the Beutler levels, $n_2^+(^2D_{5/2})$ and $n_2^+(^2D_{3/2})$ in Table 1 from n_2^+. All the results are listed in Table 2, together with all of the ionization rates n_eZ_1 and n_eZ_2. The values of n_2^+, $n_2^+(5^2S_{1/2})$, $n_2^+(^2D_{5/2})$ and $n_2^+(^2D_{3/2})$ are also given as a function of T_{ev} in Fig. 8.

From Fig. 5 and Table 2, it is seen that the calculated values of T_e at varied evaporator temperatures are nearly equal to the measured values; and that T_e decreases only a little for the increase of T_{ev} from 0 to 258°C. The latter fact is explained by the counterbalance between the increase of Cd ionization and the decrease of He ionization (see Table 2). That is, for the elevation of T_{ev}, the increase of Cd density in the plasma leads to the increase of Cd ionization, which is accompanied by the decrease of T_e. Meanwhile, the decrease of T_e causes the decrease of He ionization, which prevents the lowering of T_e.

In Table 2, it is seen that the ionizations of Cd occur predominantly by the Penning collisions with He atoms in the four lowest excited levels. Furthermore, the contribution from the ionizations by the electron collisions with Cd atoms in the 5^3P levels is a considerable amount at the elevated temperature of T_{ev}.

5-2 Excitation mechanism of the 4416 Å lower $5^2P_{3/2}$ level

The maximum absorption coefficient k_0 for Cd^+ 2144 Å line is calculated from $n_2^+(5^2S_{1/2})$, $T_i \equiv T_g = 450°C$ and the radiative transition probability of the line[12] under the assumption that the line is Doppler broadened. The product of k_0 and R, which is the optical depth perpendicular to the column, is 0.12[30], even at $T_{ev} = 258°C$. Radiation imprisonment is considered not to take place for the 2144 Å emission. In consequence, the T_{ev} dependence of the 2144 Å emission in Fig. 4 is equivalent to that of the population density n_l of the 4416 Å lower $5^2P_{3/2}$ level.

This fact supports the discussion of §2-1, that the lower level is not populated predominantly by the radiative cascadings of the 4416 Å, 3536 Å, 2748 Å and 2313 Å lines. It has been also proved from the previous measurement[3] that the lower level is not excited predominantly by the Penning collisions of the Cd ground 5^1S_0 level with He atoms in the four lowest excited levels ($i = 2$ to 5).

Table 3. Various rates ($cm^{-3}\,s^{-1}$) for population to Cd^+ $5^2P_{3/2}$ level under the same condition as in Table 2.

T_{ev} (°C)	209	229	249	258
Cascade ($5s^2\ ^2D_{5/2}$)	3.7^{16}	5.4^{16}	7.2^{16}	6.4^{16}
Cascade ($5s^2\ ^2D_{3/2}$)	4.3^{15}	6.8^{15}	8.8^{15}	8.4^{15}
e- collision (5^1S_0)	4.7^{14}	8.5^{14}	1.5^{15}	1.9^{15}
e- collision ($5^2S_{1/2}$)	5.3^{15}	1.2^{16}	2.3^{16}	2.9^{16}
Total	4.71^{16}	7.28^{16}	1.05^{17}	1.03^{17}

Now, we examine the excitations of the lower level by the electron collisions with the Cd ground 5^1S_0 and Cd^+ ground $5^2S_{1/2}$ levels. The rates for these collisional excitations are calculated and compared in Table 3, with the rates for the populations by the cascadings of the 4416 Å and 3536 Å lines under the same condition as in Table 2, where the spontaneous transition probabilities for the 4416 Å and 3536 Å lines are $1.28 \times 10^6\ s^{-1}$ and $0.52 \times 10^6\ s^{-1}$, respectively[11]. Furthermore, the rate coefficient for the excitation from the Cd ground 5^1S_0 level to the lower level is calculated from a cross section obtained in the experiment[28] and shown as a function of T_e in Fig. 7. The rate coefficient for the excitation from the Cd^+ ground $5^2S_{1/2}$ level to the lower level is calculated from the semi-empirical formula for the cross section[29], where the optically allowed hydrogenic transition is assumed. The value of the rate coefficient becomes about 1×10^{-8} cm^3/s in the energy range concerned, where use is made of the oscillator strength of 0.39[31].

In Table 3, it is seen that the total rate for the population to the lower level by the collisional excitations is smaller than the population rate by the cascading of the 4416 Å line. This fact indicates that the lower level is not excited predominantly by the electron collisions with the Cd ground 5^1S_0 and Cd^+ ground $5^2S_{1/2}$ levels.

Finally, we consider the excitation by the electron collisions with Cd 5^3P levels. As shown in Table 1, the population density of all the 5^3P levels is relatively large and monotonously increases as T_{ev} increases. The rate coefficient for the excitation from the 5^3P levels to the lower level may be assumed to be comparable to the one for the excitation from the Cd^+ ground $5^2S_{1/2}$ level to the lower level. Then, the rate for the excitation from the 5^3P levels to the lower level is nearly the same as the total rate of the cascadings. Hence, the total collisional excitation rate becomes larger than the latter. This fact supports the experimental result in Fig. 4, namely that the population density of the laser lower level increases monotonously with the increase of T_{ev}.

References

1) W. T. Silfvast; Appl. Phys. Letters, **13**, 169 (1968).
2) P. G. Browne and M. H. Dunn; J. Phys., **B6**, 1103 (1973).
3) K. Miyazaki, Y. Ogata, T. Fujimoto and K. Fukuda; Japanese J. Appl. Phys., **13**, 1866 (1974).
4) T. G. Giallorenzi and S. A. Ahmed; IEEE J. Quant. Electr., **QE-7**, 11 (1971).
5) H. B. Dorgela, H. Alting and J. Boers; Phys. Haag, **2**, 959 (1935).
6) A. von Engel and M. Steenbeck; Elektrische Gasentladungen Ihre Physik und Technik (Springer, Berlin, 1932), Vol. 2, p. 82.
7) W. Schottky; Phys. Zeit., **25**, 635 (1924).
8) R. T. Young, Jr.,; J. Appl. Phys., **36**, 2324 (1965).
9) L. Tonks and I. Langmuir; Phys. Rev., **34**, 876 (1929).
10) J. R. Fendley, Jr., I. Gorog, K. G. Hernqvist and C. Sun; RCA Rev., **30**, 422 (1969).
11) M. Barrat and J. P. Barrat; Comp. Rend., **257**, 1463 (1963).
12) S. R. Baumann and W. H. Smith; J. Opt. Soc. America, **60**, 345 (1970).
13) D. T. Hodges; Appl. Phys. Letters, **17**, 11 (1970).
14) E. O. Johnson and L. Malter; Phys. Rev., **80**, 58 (1950).
15) T. Dote; Japanese J. Appl. Phys., **7**, 964 (1968).
16) T. Dote; Rika Hohkoku, **46**, 122 (1970).
17) V. N. Kolesnikov; Physical Optics (Consultants Bureau, New York, 1966) Vol. 30, p. 53.
18) J. C. Bowe; Phys. Rev., **117**, 1416 (1960).
19) M. H. Dunn; J. Phys., **B5**, 665 (1972).
20) I. G. Ivanov and M. F. Sem; Soviet Phys.-Tech. Phys., **17**, 1234 (1973).
21) Y. Ogata and K. Fukuda; THIS MEMOIRS, **35**, 177 (1973).
22) S. C. Brown; Basic Data of Plasma Physics, Second Edition, Revised (The M. I. T. Press, Cambridge, Massachusetts, USA, 1966).
23) G. T. Collins; J. Appl. Phys., **44**, 4633 (1973).
24) A. Dalgarno; Phil. Trans., **250**, 426 (1958).

25) L. M. Chanin and M. A. Biondi; Phys. Rev., **107**, 1219 (1957).
26) R. Mewe; Physica, **47**, 398 (1970).
27) W. Lotz; Zeit. Phys., **232**, 101 (1970).
28) S. P. Varshavskii, A. A. Mityureva and N. P. Penkin; Opt. Spectr., **29**, 341 (1970).
29) H. W. Drawin; Association Euratom-C.E.A. (1967), Report No. EUR-CEA-FC-383 (revised).
30) T. Holstein; Phys. Rev., **72**, 1212 (1947).
31) T. Andersen and C. Sørensen; J. Quant. Spectr. Rad. Transfer, **13**, 369 (1973).